# Enhancing Lung Cancer Detection: A Hybrid Approach with FbAC-NET and Bi-LRCN

## Geetha K[1], Dr. Karthikeyan Elangovan[2]

[1]Research Scholar (Part time Internal), Department of Computer and Information Science, Annamalai University, Annamalai Nagar, Tamil Nadu, India.

[2]Research Supervisor, Assistant Professor/Programmer, (Deputed as Assistant Professor and Head in Government Arts and Science College, Gingee, Villupuram), Department of Computer and Information Science, Faculty of Science, Annamalai University, Annamalai Nagar, Tamil Nadu, India.

Email ID: geetha2kumar@gmail.com

Email ID: kanchikarthi2010@gmail.com

## ABSTRACT

Lung cancer remains a significant public health concern, necessitating accurate and efficient methods for early diagnosis. Traditional diagnostic techniques often rely on manual interpretation of medical images, leading to subjective results and increased dependency on the expertise of radiologists. In clinical practice, lung X-ray pictures are also periodically reviewed by field professionals. Here we propose a hybrid model that combines two powerful deep learning architectures. The first component of our model, FbAC-NET, is an advanced neural network based on the Feature-based Adaptive Convolutional Network (FbACN) architecture. FbAC-NET is designed to extract highly discriminative features from lung cancer images, enabling effective classification. Leveraging the advantages of FbAC-NET, we enhance the accuracy of lung cancer classification by incorporating the second component, Bi-LRCN (Bidirectional Long Short-Term Memory Recurrent Convolutional Network). Bi-LRCN is specifically tailored for sequential data analysis, making it suitable for capturing temporal dependencies and patterns in lung cancer progression. By combining the strengths of FbAC-NET and Bi-LRCN, our hybrid model achieves superior performance in multi-classification and detection of lung cancer. We conduct extensive experiments on a sizable dataset of lung cancer images. According to the results, our hybrid model performs superior to other methods. By automating the diagnosis process, our approach has the potential to enhance early detection rates, enabling timely interventions and improving patient outcomes. Utilising a Python experimental design, the system's effectiveness is then evaluated. In the LIDC/IDRI dataset, the suggested classifier performed with performance metrics of 99.89% sensitivity, 99.84% specificity, 99.25% precision, and 99.7% accuracy. For the other dataset the performance metrics were 99.63% sensitivity, 97.9% specificity, 97.6% precision, and 99.8% accuracy.

*Keywords:* *BI-LRCN, lung cancer, FbAC-NET, diagnosis, optimization algorithm, pre-processing, extraction.*

## 1. INTRODUCTION

One of the most common and lethal types of cancer in the world is lung cancer. By enabling prompt therapeutic approaches, early diagnosis is essential for improving patient outcomes. Traditional lung cancer diagnosis depends on radiologists' subjective and fallible visual examination of medical pictures. A specific kind of cancer called lung cancer usually develops in the cells lining the airways of the lungs. It kills more people than any other factor associated to cancer globally, killing both men and women. Non-small cell lung cancer (NSCLC) and small cell lung cancer (SCLC) are the two primary subtypes of lung cancer, with NSCLC being the more prevalent. Smoking, second hand smoke exposure, occupational exposure to toxins like asbestos and radon gas, a family history of lung cancer, and certain genetic mutations are all risk factors for developing lung cancer. Lung cancer is almost always caused by smoking tobacco, and the risk rises with time and quantity of smoking. Lung cancer symptoms might range, but may include hoarseness, recurrent coughing up blood, exhaustion, weight loss, chest discomfort, and shortness of breath. Lung cancer, however, typically does not present with obvious symptoms in the early stages, making early identification difficult.

Medical imaging, including chest X-rays, CT scans, and PET scans, as well as tissue samples for histological analysis are frequently used to make diagnoses. The staging of lung cancer aids in estimating the severity of the condition and directs therapy choices. The kind and stage of the disease, as well as the patient's general condition, all influence the available

treatments for lung cancer. Surgery, radiation, chemotherapy, targeted treatment, and immunotherapy are a few examples. Oncologists, surgeons, radiation oncologists, and other medical specialists frequently collaborate to decide on a course of therapy, including other healthcare practitioners. The stage of the disease at diagnosis, the kind of lung cancer, the existence of certain genetic abnormalities, and the patient's general health all have a significant impact on the prognosis for lung cancer. The highest prospects of favourable results and long-term survival come from early identification and treatment. The main goal of lung cancer prevention is to minimise or completely avoid exposure to risk factors, especially tobacco smoke. This entails giving up smoking, staying away from smoke in public places, and limiting exposure to environmental and occupational carcinogens. The use of low-dose CT scans in lung cancer screening programmes is advised for people who are at a high risk, such as lifelong smokers.

This study suggests a hybrid strategy that combines the strengths of the FbAC-NET and Bi-LRCN deep learning architectures. This hybrid system attempts to enhance lung cancer diagnosis by efficiently using spatial and temporal information from lung pictures and videos by combining the advantages of both designs. The proposed system's FbAC-NET component uses CNNs with attention methods to extract pertinent characteristics from lung pictures. CNNs are excellent at identifying local characteristics and spatial patterns, which makes them perfect for analysing medical pictures. The network can focus on the most useful sections of the lung pictures thanks to the attention mechanisms, which improve the identification process by emphasising regions that are more likely to contain malignant cells. By combining these techniques, FbAC-NET provides a powerful feature extraction tool that can improve the accuracy of the model.

In addition to spatial analysis, the proposed hybrid approach also incorporates temporal analysis through the Bi-LRCN component. This component is specifically designed to process sequential data, such as lung tissue motion captured in videos or sequential scans. By utilizing bidirectional processing, Bi-LRCN can analyze the spatiotemporal patterns in the lung data, capturing both past and future context. This capability enables a deeper understanding of cancer-related changes over time, potentially improving the detection of subtle abnormalities that may not be evident in individual static images.

Thus, the proposed hybrid approach that combines FbAC-NET and Bi-LRCN offers a promising solution to enhance lung cancer detection. By leveraging spatial and temporal information from lung images and videos, this hybrid system aims to improve the accuracy, efficiency, and early detection of lung cancer. For appropriate treatment interventions to be made and for patient outcomes to be improved, early and accurate lung cancer identification is essential. The detection of lung cancer might be revolutionised by applying deep learning methods to the field of medical imaging, which would be advantageous to both patients and medical professionals.

## 1.1 Motivating factors and problem-solving

DL-based computational imaging techniques help identify cancer by utilising image processing technologies. It is necessary to reduce accuracy, improve classification accuracy, and reduce mistakes in medical diagnosis. Another issue is how to maintain global coherence among the several entities involved in network structure and integrated design of solutions.

Lung cancer stands as a profound global health concern, marked by its high mortality rates and late-stage diagnoses. Early detection of lung cancer is pivotal in improving patient outcomes and reducing the burden on healthcare systems. Traditional diagnostic methods, which rely heavily on manual interpretation of medical images, are fraught with subjectivity and dependency on the expertise of radiologists. Moreover, they may not fully capture the evolving nature of the disease over time. The motivation here is to develop an objective and consistent approach that reduces diagnostic subjectivity, to capture these temporal aspects for a more comprehensive understanding of the disease, and to contribute to the broader goal of improving healthcare outcomes.

This study will provide a hybrid framework that combines two optimisation methods based on the earlier discussion. A strategy for picking the optimal subset of characteristics is necessary to boost the performance of the framework. Because selecting the appropriate subset of features is an NP-hard problem, it is desirable to employ metaheuristic methods.

## 1.2 Proposed models contributions

This article provides an automated computer-aided approach for identifying lung cancer to solve the concerns stated above. Initially, a pre-processing stage that helps with picture noise suppression is part of the proposed system. The lung cancer spot is then separated from its surrounds using a segmentation approach. The phase of feature extraction is where the collection of morphological, texture, brightness, or statistical characteristics for the detected objects is formed. This article suggests a novel model for lung tumour prediction based on a hybrid Bi-LRCN algorithm to address these problems. The optimisation Method's convergence rate is increased by combining Bi-LRCN and ChoA.

- ➢ The proposed model, which incorporates the benefits of both the hybrid FbAC-NET and the Bi-LRCN models, shows an immense enhancement.
- ➢ To improve the image quality, pre-processing is performed.
- ➢ Chimp optimization algorithm (ChOA) is developed for improving the efficiency of the model. In our proposed lung tumor classification, ChOA is used as the optimization technique.

- In this research work, a hybrid algorithm using CT of lung images was used to detect and classify the tumour.
- Theoretical effectiveness of the proposed algorithm is presented.
- The proposed approach is compared to existing algorithms via experimental analysis.
- The total efficiency of the hybrid FbAC-NET and Bi-LRCN obtained 99.68%.
- On the chest X-ray dataset and the LIDC/IDRI dataset, the suggested model yields the best results.

**1.3 Paper organisation**

The arrangement of our paper is as follows: Section 2 examines a review of the approach that is currently in use. Section 3 presents the suggested model, while Section 4 describes simulation and discussion. The flaw in our suggested model is noted in section 5. Section 6 is where the paper is concluded.

## 2. RELATEE2D WORK

AdaBoost & DenseNet algorithms [21] and lung cancer detection forms have been identified along with automated classification methods. This method was considered one of the greatest techniques for pathology-type lung cancer and acted as non-invasive and very effective.

CT images lung cancer detection has been identified by using some of the hybrid approaches one such Hybrid approach named ODNN [22] along with LDA also with the MGSA.

*In 2019, Huseyin Polat and Homay Danaei Mehr et al.,* have introduced an effective diagnosis for lung cancer named a three-dimensional CNN-based conventional softmax and also a three-dimensional based Radial Basis Function (RBF) [23] which was on the basis of a Support vector machine.

A method [24] called changeable texture-based CNN which was utilized for extracting the feature and it was completely an energy layer rather than just a pooling layer. The recommended model was utilized to enhance the performance of lung cancer in the pulmonary nodules classification inside the CT scanned images. The dataset utilized for the classification process was LIDC-IDRI also it was executed on LUNGx. Moreover, it yielded an accuracy of 96.69% overall.

The automated diagnosis of lung cancer using two-dimensional CNN networks and Taguchi parametric optimisation was described [25]. Additionally, a collection of datasets from the International Society for Optics and Photonics (SPIE-AAPM), Lung Image Database Consortium, and Image Database Resource Initiative (LIDC-IDRI) were used for analysis.

A system called Adaptive Hierarchical Heuristic Mathematical Model [26], abbreviated as AHHMM, for evaluating Non-small Cell Lung Cancers that generated a 96.67 percent accuracy.

A Fuzzy based Particle Swarm Optimization along with Convolutional Neural Network (FPSOCNN) [27] in order to effectively classify and identify lung cancer nodules. However, this model had been included with some of the extraction techniques as well, they were: Local binary patterns, Wavelet transform also Scale Invariant Feature Transformation (SIFT).

A comprehensive diagnosis of lung cancer has found a 3D-based CNN nodule detector [28] and an RNN-based hierarchal nodule detector. Here, the model was incorporated with two cascaded modules, one was the module of risk evaluation, and the other one was the module with nodule detection.

In lung cancer lesions, the given DL-enabled SVM CAD model [29] recognises physiological and pathological alterations in soft tissue cross-sections. The programme is originally taught to diagnose lung cancer by comparing and contrasting possible characteristics in CT scans collected from patients and influence persons at the time of diagnosis.

The LCGANT hybrid architecture was created in 2022 by Ren et al. Two distinct elements make up their design. To create fake pictures of lung cancer, deep convolutional GAN (LCGAN) was employed. To divide lung cancer pictures into three groups in the second part, the VGG-DF regularization-enhanced transfer learning model was applied. Pictures from both real and made-up sources may be found in the VGG-DF collection. An overview of the literature review may be seen in Table 1.

**Table 1 summarises the detection and categorization of lung cancer.**

| Authors[Citations] | Findings | Drawbacks |
|---|---|---|
| [21] | AdaBoost algorithm and DenseNet | Not Optimize the Hyper Parameters. |
| [22] | Optimal Deep Neural Network | Unsuitable for backgrounds with more than three distinct complexes. |
| [23] | hybrid 3D-CNN- RBF | No hybrid algorithms. |

| [24] | CNN | Hardly Appropriate for Personalised Health-Care Connected Large-scale applications including personalised health care are not feasible. |
|------|-----|-----|
| [25] | 2D Convolutional Neural Network | Unfit for the Complex Patterns Dataset. |
| [26] | Mathematical Model with Adaptive Hierarchical Heuristics | No DL architectures that are broad and deep. |
| [27] | CNN with fuzzy particle swarm optimisation | Maximum Loss Function. |
| [28] | Nodule detector based on 3D-CNN and hierarchical RNN | Absence of hybridization algorithm. |
| [29] | Support vector machine | No prediction for trained data. |
| [30] | LCGAN | The training would be extremely slow with a subpar GPU. |

## 2.1 Survey

The section that follows discusses the many approaches and categorization systems for lung cancer. Even if there are a few study gaps that need to be filled. For the method of classifying and diagnosing lung cancer in [23], a hybrid deep learning technique is utilised. In [16] it does not account for cancer variation. Therefore, this paradigm is unable to express intricate patterns. Although CNN was employed in [17] the hyper parameters were optimised. The idea of edge cloud computing is also inappropriate. [14] use a DCNN approach for classifying lung cancer because utilising the proposed strategy to minimise the highest likelihood loss function does not produce better outcomes.

## 3. PROPOSED METHOD

For the purpose of diagnosing the condition and selecting a course of treatment, lung cancer must be classified. On the other hand, CT scan is widely used because to its improved picture quality and lack of ionising radiation. Deep learning (DL), a subfield of machine learning, has lately demonstrated outstanding performance, notably in classification and segmentation problems. Figure 1 depicts the recommended approach diagram. The four stages of the cancer prediction technique described in this study are pre-processing, segmentation, feature selection, and classification. The acquisition of lung CT imaging is followed by transmission of the images to the top-hat filtering-based pre-processing stage. After pre-processing, the CT image and the picture are separated using lesion segmentation. The step of feature selection uses the output of the image segmentation process.
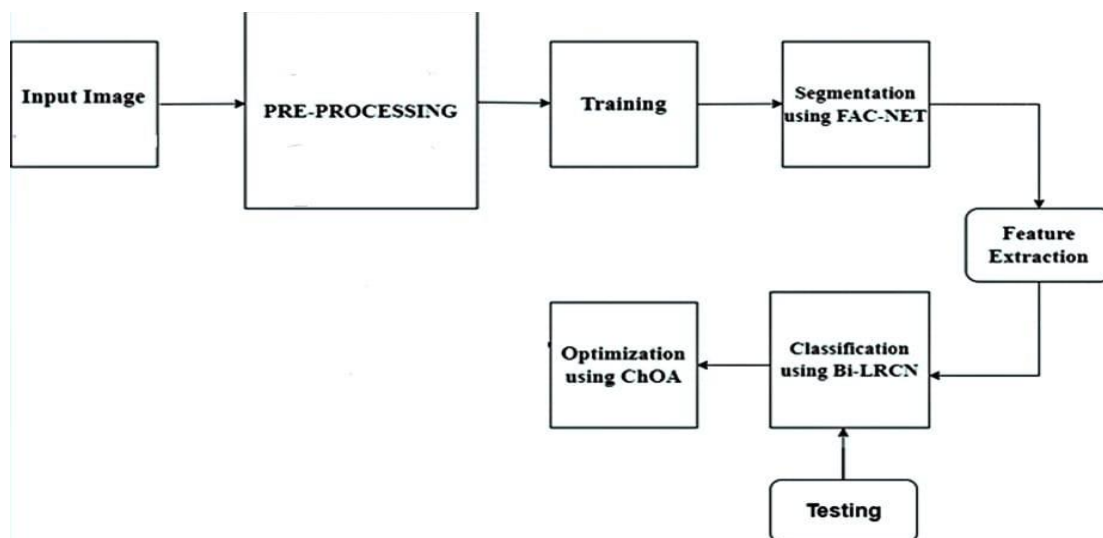


**Fig 1: Proposed Model**

Geetha K, Dr. Karthikeyan Elangovan

The suggested model's workflow is depicted in Figure 1, where the input picture is obtained from the dataset. Next pre-processing phase take place, where image filtering and contrast enhancement take place, after pre-processing the model is trained and segmented using FbAC-NET algorithm. Once segmentation is completed, the features are extracted by window sliding and shape based extraction technique. After that, the trained data is tested at the classification stage, here for classification model Bi-LRCN technique is used. The final step is to optimize the classified output and to improve the correctness of the prediction type. At last, the tumor types are classified. The detailed explanation of each block is explained in detail as follows.

### 3.1 Pre-processing

In preparing the image medical data for this study, Images were formatted to appropriately pre-procesed before transmitting to the model, so that images can be easily read from the file. Both image random flipping and random zooming were carried out. Images that formerly had values between 0 and 255 were scaled in order to have values between 0 and 1.

### 3.1.1 Filtering Technique

Image filtering is a technique used to enhance the clarity and readability of CT scans. It is frequently employed to lessen the influence of visual noise and improve the visibility of tiny structures or details. CT images may be processed using a number of image-filtering technologies. To improve the raw image, noise reduction using bicubic interpolation (BI) is applied in this study. Using the Bicubic Interpolation method, a high-resolution image may be created from a low-resolution one. The guided, Gaussian, top-and-bottom-hat, and median filters are used to reduce noise and smooth the image.

---

**Algorithm:** Image Enhancement with Top-Hat and Bottom-Hat Operations

**Step 1: Initialization**

$$I(i, j) \leftarrow a\_ij * x\hat{}i * y\hat{}j \qquad\qquad (1)$$

I(i, j) - Image at location

a_ij - Low-resolution image

x^i * y^j - High-resolution image

**Step 2: Image Enhancement**

Perform Gaussian filtering on I to get I_guassian.

Calculate I_Tho (Top-Hat Opening):

$$I\_Tho \leftarrow I\_guassian - (I\_guassian \otimes \theta\ strel) \oplus strel \qquad (2)$$

Calculate I_Bhc (Bottom-Hat Closing):

$$I\_Bhc \leftarrow (I\_guassian \oplus strel)\ \theta\ strel - I\_guassian \qquad (3)$$

Calculate I_(Th-Bh):

$$I\_(Th\text{-}Bh) \leftarrow I\_guassian + I\_Tho - I\_Bhc \qquad (4)$$

Calculate I_enhance:

$$I\_enhance \leftarrow I - I\_guassian + I\_(Th\text{-}Bh) \qquad (5)$$

Update I:

---

I ← I_enhance          (6)

**Step 3: Sharpening**

Calculate Laplacian Gradient:

I_laplacian ← I_(grad X) + I_(grad Y)          (7)

I_(grad X) - Image gradient in the X-direction

I_(grad Y) - Image gradient in the Y-direction

I_sharpen ← I_enhance - C * I_laplacian          (8)

C - Multiplicative coefficient

### 3.1.2 Phase of contrast enhancement

The contrast enhancing technique known as adaptive histogram equalisation is used after removing noise from datasets.

$$contrast(i, j) = rank * \max\_ \text{int} \, ensity(i, j) \therefore Initially \, rank = 0 \tag{9}$$

The new leading row's trailing column is eliminated, and the preceding row's primary position is utilised to generate the histogram in each line's major position. The limitation must be established and the image's complexity must be raised. Figure 2 shows both the unfiltered and filtered versions of the image.
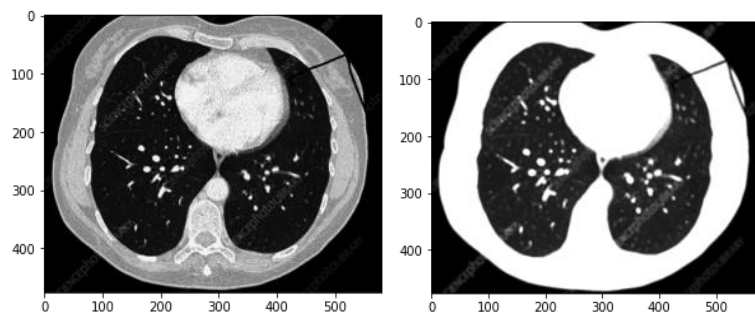


**Figure 2. (a) Input dataset image**          **(b) Pre-processed image**

### 3.2 Segmentation Model

The visual representation is frequently modified and made simpler by the segmentation job to make it more understandable. To create groups, the programme selects comparable pixels. Cancer is segmented using an unsupervised method, with segmentation results utilising the provided group values. The initialized equation is given as, $\sum_{i=1}^{5} C_i \leftarrow 1$.

$$f_{\mu i} = C \sum \frac{X_i}{N} \tag{10}$$

$$f_R = \beta - \alpha \tag{11}$$

$$f_{\partial} = \frac{R}{C_i} \tag{12}$$

$$f_{\vartheta_{\partial i}} = \partial + 1 \tag{13}$$

$$f_{\omega} = \theta(K_0 \rightarrow \vartheta) \tag{14}$$

$$f_{\omega} - \text{image centroid;}$$

Then, the variation between all of them $\omega_j$ and all other centroids are estimated, and updated as in Eq. (15) and Eq. (16)

$$f_{\omega_j} = \sum_{i=0}^{n} \omega_i - \omega_j \tag{15}$$

$$f_{\vartheta \omega j} = \sum_{i=1}^{5} C_i + (i + 1) \tag{16}$$

The final segmentation value of binary data $(f_{binary})$ value is given in eq. (17)

$$f_{binary} = f_{\vartheta_{\omega\mu j}}(\Sigma \frac{X_i}{N}) \qquad (17)$$

$f_{\vartheta_{\omega\mu j}}$ − Mean value of particular updated cluster;

The segmented image $(f_{seg})$ is created as shown in Eq (18)

$$f_{seg} = f_{binary} \otimes f \qquad (18)$$

Lung tumour segmentation refers to the method of differentiating between the diseased and normal parts of a patient's lung using artificial or other means, and then precisely segmenting the affected part to be get ready for the physician's upcoming evaluation and therapy. Segmentation based on thresholds, edge detection, region growth, and active contours approaches are examples of traditional lung tumour segmentation algorithms [24]. These classic procedures are still used successfully in medical pictures. Since deep learning has advanced in field of computer in recent times, a huge number of experts and academics are actively investigating its application in a variety of fields, including lung tumour segmentation. It achieved outstanding success in lung tumour segmentation.

### 3.2.1 (FbAC-NET) Feedback attention network

The proposed segmentation of lung network design, FbAC-Net, which is based on Context encoder network CtE-Net, is depicted in the figure. The network, in particular, serves as the foundation of the FbAC-Net network. The feedback fusion block (FFB), which allows the system to collect affluent feature data throughout the downsampling stage, was then implemented.

An attention mechanism (AM) phase is utilized in the upsampling stage to extract crucial data from the feature map's large amount of data. In comparison to the formerly suggested Attention Gate (AtG) block, which generates the attention weight map directly from the worldwide data at the hop link. At last, the result of each layer was weighted using the weight plot that was created. The proposed network has the unique feature of combining the concepts of attention module weighting and feedback fusion to reuse the feature map and emphasise the important information [25]. These two concepts are utilized in the data affluent down-sampling block and the up-sampling. In figure 3, there are, three Feedback Fusion (FbF) blocks, three Attention mechanism (AM) block, and a single extraction of context block.
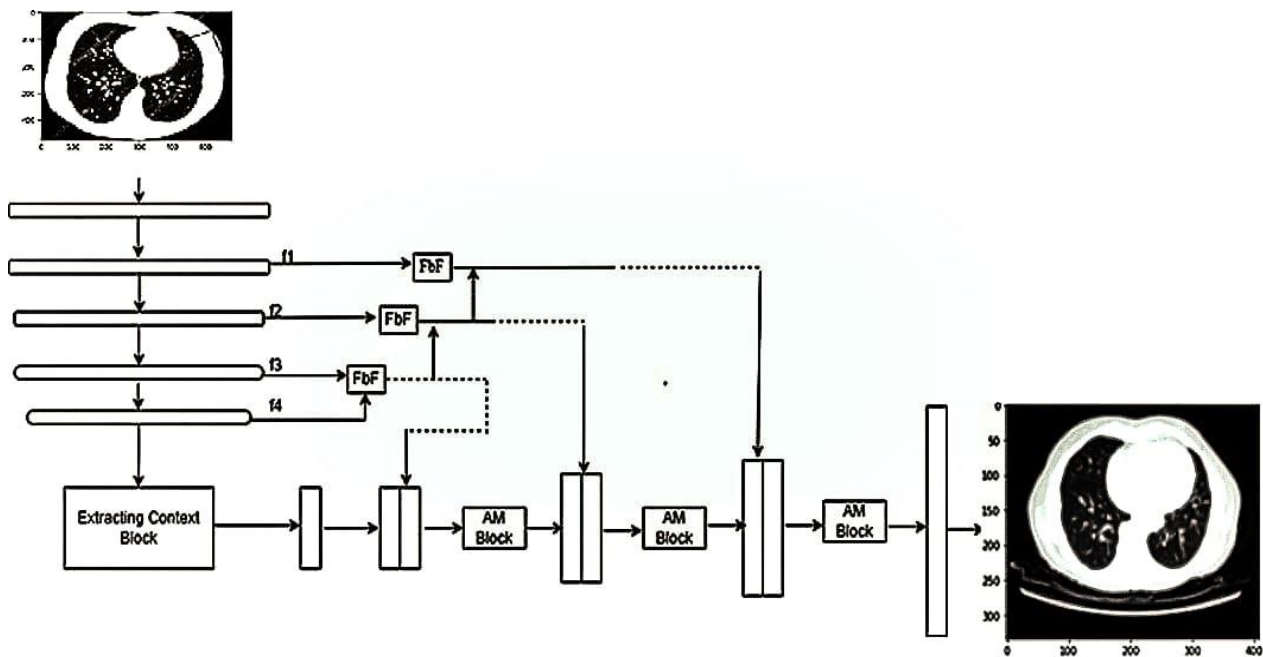


**Figure 3- The overall design of FbAC-Network**

### 3.2.1.1 Feedback Fusion Block (FFB)

Encoding and decoding structures are commonly employed in deep learning frameworks to retrieve map characteristics. Pooling and convolution modules are included in the down sampling part. While performing the pooling and convolution functions, the system will keep on getting featured data from the incoming data. However, the system will miss or lose some

important feature information while performing the extraction. Because of the significant complexity of lung tumour, it is especially important to obtain global information while dealing with the gathering of lung tumour images. As a result, reducing the loss of essential information has become a pressing issue for us to address. This study proposes a solution to this practical difficulty. The feedback technique can make use of previously used parameter data to produce stronger feature data. As this is a research issue lacking data enrichment, it is essential to utilise features extracted from datasets in the networking in order to get knowledge that is similar to the enhancement of data [26]. As a result, this work offers a novel and effective FFB module that is driven by the feedback mechanism. In earlier research, the feature pyramid network (FePN), uses an up-down network topology with wide extent to produce accurate prognosis on every layer of extracted features, the reuse of features also takes place. Each layer's output feature maps are sampled up by the previous layer's output maps. The FbF block suggested in our work, however, is differ from the other network [27]. To acquire the result of each layer's after FbF, top-down feedback is used to feed back the top-level feature information to the bottom-level and in the up-down feedback direction, respectively. In particular, the FFB module receives feature data from two adjacent downsampling layers, which is then combined with equivalent upsampling layers through a skip connection. This method of processing get more relevant feature information to the lung tumour without changing the extraction operation. Simultaneously, Experiments have shown that the FbF block can significantly boost the segmental impact of lung tumours. FbF, in particular, is made up of two input components [28].

### 3.2.1.2 Attention Mechanism Block

By lowering the number of parameters, feedback fusion modules in our study have a positive effect on the reuse of models boundary. Nevertheless, as all of these structures transmit feature information through iterative training rounds. During rounds, duplicated features data in addition to certain noise can have an additional effect and harm network convergence as well as the output. Researchers renamed the CBAM attention module the AM module, which has the same structure as the CBAM module, as part of this study enhancement to counterbalance the negative effects generated by FFB modules. Due to the substantial amount of similarity among multi-channel extracted features used in network design, critical feature information is most frequently occurring feature information in each channel at the same time (that is, what we need to acquire) [29]. As a result, this study indicates that to improve Sam's ability to screen important feature information, Sam modules will be given an algorithmic branch that solves mode values. The structure is depicted in Figure 3.

### 3.3 Extraction of feature

A crucial stage in the classification process for image processing is feature extraction. Due to its enormous size, the complete image is typically minimized to a set of attributes that can be further examined. The quantized volumes are used for both image pre-processing and the extraction of statistical texture-features. The aim of the feature extraction approach is to represent the picture as a set of single values or vectors of matrices, which is its most fundamental and identifiable form. A more manageable collection of qualities must be derived from the incoming data [30]. The characteristics are assigned to the class they stand for by the classifiers after receiving the qualities as inputs. By predicting beneficial features, feature extraction seeks to decrease the amount of data. Here, the extraction method is based on form and uses window sliding.

### 3.3.1 Sliding window operation

Window sliding feature extraction can be used with other feature extraction techniques, including shape-based features, to improve the accuracy of lung tumour classification. The window size and overlap depend on the specific problem at hand as well as the imaging technique being used. With a smaller window size, the number of windows and computational complexity of the feature extraction process may both increase. The term "2DCNN" refers to the convolution kernel to preserve the spatial characteristics of each frames. While this can aid in the identification of tumours in an image, our current goal is to identify cancers in varying degrees, which necessitates a large number of frames in a sequence. Time Distributed wrappers can concentrate on temporal information instead of having to train the model's stream for each image, which takes a large amount of computing time. The convolutional network's spatial characteristics may be extracted while keeping the temporal feature well preserved thanks to the Time Distributed wrapper, which permits the encapsulated CNN levels to be deployed to every input time slice. We used convolution-pooling-convolution-pooling to extract features from the data, allowing for more nonlinear changes than was possible with VGG16 [31]. In the CNN component of the model, we used convolutional kernels for extraction of features, which unavoidably deepens the network.

### 3.3.2 Shape based extraction

Shape-based extraction is a technique used to extract features from the shape and geometry of objects in imaging data, such as lung tumors. Here are some common shape-based features used in lung tumor classification

Volume: The volume of a lung tumor is a simple and intuitive feature that can be extracted from imaging data. It can be calculated by summing the voxel values within the tumor boundary.

Surface area: The surface area of a lung tumor can be used to characterize its extent and shape.

Sphericity: The sphericity of a lung tumor is a measure of how closely it approximates a sphere.

Compactness: The compactness of a lung tumor is a measure of how tightly packed its voxels are.

Eccentricity: The eccentricity of a lung tumor is a measure of how elongated or flattened it is. It can be calculated using the eigenvalues of the moment of inertia matrix of the tumor.

Symmetry: The symmetry of a lung tumor can be used to distinguish between different types of tumors. It can be calculated by comparing the mirror images of the tumor.

Fractal dimension: The fractal dimension of a lung tumor is a measure of its complexity and irregularity. It can be calculated using methods such as box-counting and Minkowski-Bouligand dimension.

Shape-based features can be used alone or in combination with other feature extraction techniques to improve classification performance in lung tumor classification.

### 3.4 Classification

The chosen features are delivered to the classification stage after the feature extraction phase. In this study, a Bi-LRCN is utilised to categorise the input picture sub categories.

### 3.4.1 Bi-LRCN

The Bi-LRCN is a deep learning network that combines the LSTM with CNN. It is an aggregation network for processing sequential inputs and outputs, since it is capable of handling periodic video or single-frame image inputs, in addition to single-value predictions and temporal prediction. In tasks like activity recognition, image and video description, among others, bi-LRCN is commonly used. The performance of Bi-outstanding LRCN has resulted in improvements. To create the Bi-LRCN for learning engagement recognition, a 2-Dimensional CNN packed by a Time Distributed layer and BiLSTM are merged. A Bi-LRCN model employs two independent RNNs to process the input sequence both forward and backward [32]. The output of the two RNNs is then blended using a merge layer to form the Bi-LRCN model's final output. The benefit of adopting a Bi-LRCN model over a standard unidirectional RNN is that it can capture dependencies in both directions, which can increase the model's performance on tasks like recognition and natural language processing.

### 3.5 Optimization

After categorising the model, an optimisation approach is utilised to increase the efficiency and accuracy of the suggested model. In our model, a brand-new algorithm called the Chimp optimisation algorithm (ChoA) was created using inspiration from nature. This tactic was inspired by chimpanzees' sexual drive and individual cleverness during group hunting. Compared to other social predators, it is unique. Four different phases have been utilised in this methodology to simulate various types of intelligence. The numerical description of this proposed method is as outlined below: The mathematical equations ((19)-(20)) below depict the driving and chasing of the target or prey.

$$D = \left| z.q_{prey}(n) - xa_{CHIMP}(n) \right| \tag{19}$$

$$a_{chimp}(n+1) = q_{prey} - q.d \tag{20}$$

Where z, x, and q are the coefficient vectors. Calculation of the coefficients q, z, and x by equation (21),

$$q = 2.l.rv_1 - 1$$
$$z = 2.rv_2$$
$$x = CHOTIC_{value} \tag{21}$$

Where, $rv_1$ and $rv_2$ are the random variables in range of [0, 1], $x$ denotes the chaotic vector, and l is the minimized non-linearly through the iteration process.

The mathematical behaviour of the chimps has been implemented in this step. Here, it is assumed that the initial response may be given by the attacker, driver, barrier, and chaser since they have more information about the target's position.. The remaining chimps are made to update their own positions in accordance with the best chimpanzee locations in the following iteration when four additional optima solutions have been acquired and are kept. The following mathematical equation (22)–(25), serves as an example of this process.

$$d_{barrier} = \left| z_1 q_{barrier} - x_1 y \right| \tag{22}$$

$$d_{barrier} = |z_2 q_{barrier} - x_2 y| \qquad (23)$$

$$d_{chase} = |z_3 q_{chase} - x_3 y| \qquad (24)$$

$$d_{drive} = |z_4 q_{drive} - x_4 y \ | \qquad (25)$$

When the random vectors occur within the region of [1, 1], the future position of a chimp may vary somewhere between its current spot and that of the target or prey.

$$y_1 = q_{attack} - q_1.d_{attack}$$
$$y_2 = q_{barrier} - q_2.d_{barrier}$$
$$y_3 = q_{chase} - q_3.d_{chase}$$
$$y_4 = q_{driver} - q_4.d_{driver} \qquad (26)$$

The following mathematical formula updates the chimps' location during the search procedure from the general equations Eq. (27),

$$y_{n+1} = \frac{y_1 + y_2 + y_3 + y_4}{4} \qquad (27)$$

Furthermore, the preceding mathematical expression (28) was utilised to modify the location of the chimps throughout the search process in the search domain.

$$q_{CHIMP}(n+1) = \begin{cases} q_{prey}(n) - y.d, if \phi < 0.5 \\ CHAOTIC_{Value}, if \varphi > 0.5 \end{cases} \qquad (28)$$

The chimp optimization algorithm can also be used to optimize the placement of roadside infrastructure, such as wireless access points or communication relays, to ensure that vehicles are always within range of a reliable communication signal. In vehicular communication networks, conditions such as network congestion or changes in vehicle speed may significantly affect the effectiveness of the communication network. By using chimp optimization, the network can quickly adapt to changing conditions and optimize communication routes accordingly

**Table 1 Pseudo-Code of the ChOA based Bi-LRCN Algorithm**

| |
|---|
| *Input: Training data* |
| *Output: Testing the model* |
| *Input:* |
| *- X_train: training data (a list of sequences of features)* |
| *- y_train: training labels (a list of sequences of labels)* |
| *- X_test: test data (a list of sequences of features)* |
| *- y_test: test labels (a list of sequences of labels)* |
| *- num_features: number of features in each input sequence* |
| *- num_classes: number of output classes* |
| *- seq_length: length of each input sequence* |
| *- num_epochs: number of training epochs* |
| *# Define Fbac-Net layers* |
| *fbac_net = Sequential()* |
| *# Define Bi-LRCN layers* |
| *lstm_units = 128* |

```
lstm_dropout = 0.5

model = Sequential

model.add(Bidirectional(LSTM(units=lstm_units, return_sequences=True, dropout=lstm_dropout))

# Compile the model

# Train the model

model.fit(X_train, y_train, batch_size=batch_size, epochs=num_epochs, validation_data=(X_test, y_test))
```

Our ChOA algorithm commences with a vital component, the FbAC-Net. FbAC-Net is designed to meticulously extract highly discriminative features from lung cancer images. These features serve as the foundation for effective classification and contribute to reducing the subjectivity associated with manual interpretations. FbAC-Net is tasked with scrutinizing the intricacies of medical images to identify pertinent patterns and structures. The Bi-LRCN component, occupies a central role within the ChOA algorithm. It is purpose-built for the analysis of sequential data, making it eminently suitable for capturing temporal dependencies and patterns in lung cancer progression over time. This temporal analysis capacity is pivotal in recognizing the dynamic and evolving nature of the disease. The true innovation of our approach lies in the seamless integration of these two components: FbAC-Net and Bi-LRCN. The Feature-based Adaptive Convolutional Network supplies its proficiency in image analysis, while the Bi-LRCN adds a temporal dimension to the analysis, resulting in a comprehensive understanding of lung cancer patterns.

## 4. SIMULATON DISSCUSSION

This section gives the findings of the performance evaluation of the proposed strategy. We begin by providing the two most recent datasets for lung cancer detection. Image datasets from CT scans and X-ray are utilised to characterise the created model's step-by-step operation. To examine the research findings, we must first compare the system's performance to well-known classification algorithms [33], [34], [35], [36], [37], [38], [39], [40], [39], [41], and [42]. Table 2 shows the simulation system's surroundings.

**Table 2. Setup for Simulation**

| Setup | Environment |
|---|---|
| Language | Python |
| Operating system | Windows -10 |
| processor | i7 |
| Space | 32 Giga Bytes |
| graphics | 1080ti |

### 4.1 Dataset Description

### 4.1.1 Dataset 1: LIDC/IDR

The LIDC/IDRI [31] method was used in this work (see https://wiki.cancerimagingarchive.net/display/Public/LIDC-IDRI). For training and testing, the benign and malignant portions of the picture are identified using the lung image database consortium (LIDC/IDRI) database. The LIDC/IDRI collection includes the 1018 CT cases that have undergone evaluation. Four qualified thoracic radiologists assessed each of the 1018 CT scans from the LIDC/IDRI dataset and divided the lesions into three groups: "nodule > or = 3 mm," "nodule 3 mm," and "non-nodule > or = 3 mm. "More malignant lesions than lesions in the other two groups have nodules that are < 3 mm in size.  The test dataset for this approach contains nodules in the same percentage that make up the training dataset. Figure 5 displays a few illustrations.

**(a) Normal Set**



**(b) Abnormal Set**
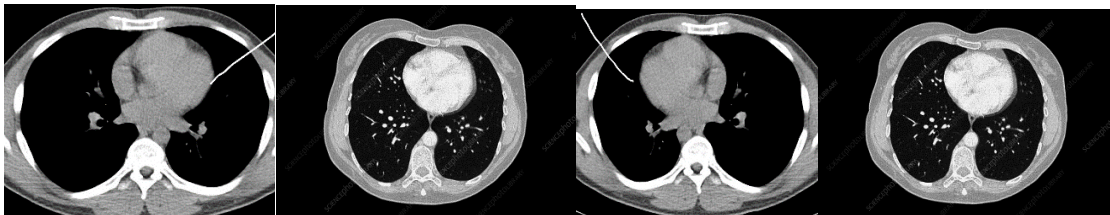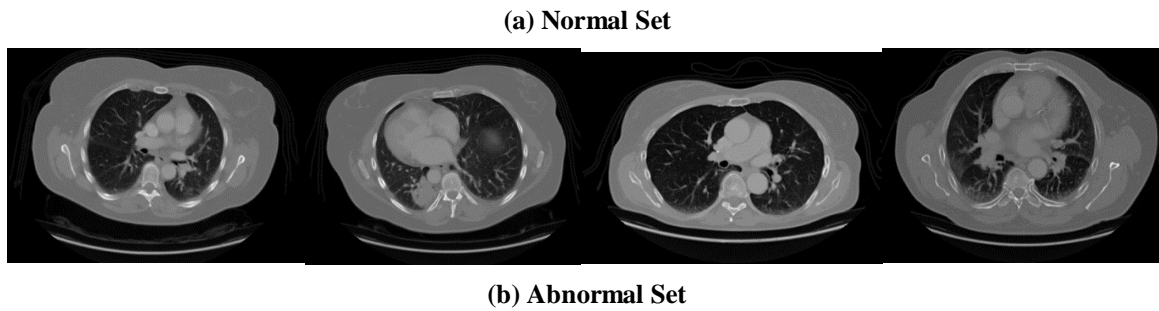
**Fig 5. Sample dataset Images**

### 4.1.2 Dataset 2: Chest X-ray

A dataset of 5856 frontal chest X-ray pictures is used in this investigation. The resolution of the photos in the collection ranges from 712x439 to 2338x2025 pixels. There are 4273 examples of rare situations and 1583 pictures of typical cases in these pictures. A selection of the collection's X-ray photographs are shown in Figure 6. Table 3 displays the data distribution for the proposed model for the training, validation, and testing stages. In our models, the normal class is denoted by 0, while the aberrant class is denoted by 1.

**Table 3. Dataset Distribution**

| Classes | Training | Validation | Testing |
|---------|----------|------------|---------|
| Normal | 1350 | 235 | 235 |
| Abnormal | 3880 | 400 | 400 |
| Total | 5230 | 635 | 635 |



**(a) Normal Set**



**(b) Abnormal Set**

**Fig 6. Sample dataset images**

### 4.2. Findings and Analysis

The input images are pre-processed, split, feature-selected, and classed to decide whether they are normal or aberrant. In this work, deep learning techniques for lung cancer diagnosis, such as Bi-LRCN and FbAC NET, are applied. The evaluation criteria demonstrate that the proposed hybrid optimisation approach, which fuses FbAC NET with deep learning, gives better

performance. This experiment also makes use of a variety of hyperparameters, including epoch 100, batch size 32, and learning rate 0.0002. Here, the output layer activation function is sigmoid and the hidden layer activation function is ReLU.

**Table 4. Parameter Settings**

| Tuning parameters | Bi-LRCN |
|---|---|
| Size of Batch | 32 |
| filters | 256 |
| Size of Step | 18 |
| Learning Rate | 0.0002 |

### 4.2.1 Image Pre-processing

Image filtering and histogram equalisation were used in the original processing of the CT or X-ray pictures. By uniformly distributing the bright and dark areas of a histogram, histogram equalisation can improve the quality of a picture. In numerous following processing steps, segmenting lesions is a key step. The full classification of typical and abnormal CT and chest X-ray imaging types is provided in Tables 5 and 6, respectively. The second column of this table clearly identifies the photo input, while the third column displays the pictures that were captured during the pre-processing phase. The improved photos are shown in the fourth rows of photographs.

**Table 5 Results of pre-processing the LIDC-IDR dataset.**
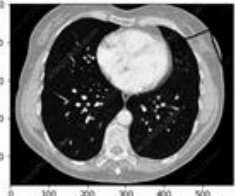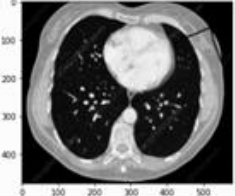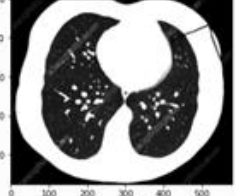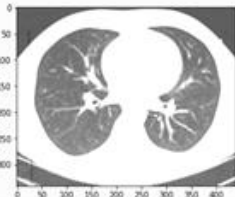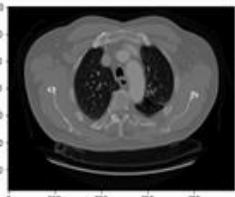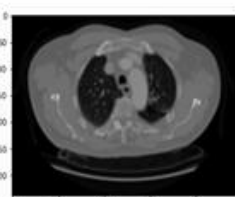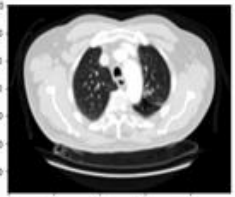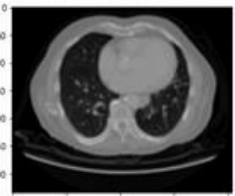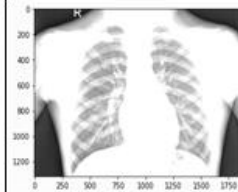
**Table 6. Outcomes of pre-processing in dataset of chest X-ray**



### 4.3.2 Chest X-ray dataset augmentation using images

The process of "data augmentation" entails altering existing data samples in order to artificially increase the size of a dataset. Data augmentation may be used to generate new chest X-ray images by performing modifications such as rotation, scaling, and inversion. This may enhance the performance of DL models by avoiding over-fitting and enhancing the model's resiliency to data fluctuations. In addition, data augmentation may be used to generate synthetic samples of regular or irregular instances, that could be beneficial for training models to identify a particular illness or condition. The photographs were randomly zoomed in to a ratio of 0.2 percent using the zoom range and then flipped horizontally. These processes contributed to the improvement of the system's precision since the input pictures might have varying angles, widths, and heights. Hence these pre-processing approaches account for such factors. The results for the augmentation of X-ray images are seen in table 7.

**Table 7. Augmentation results**

### 4.3.3 Confusion matrix analysis of the proposed approach

The results of the prediction rate of binary classes using confusion matrices on various testing samples are shown in Figures 7 and 8. Therefore, a 2 by 2 confusion matrix is used. The true class values are listed in the columns, while they are shown in the rows. The diagonal cells display the overall number of successfully categorised observations. The cells that are non-diagonal demonstrate how the observations were misclassified. Each cell totals all observations. The predicted values for each class that are marked properly and wrongly are listed in the far-right column of the confusion matrix. . These figures are sometimes referred to as accuracy (positive predictive value) and false alarm rate, respectively. The fraction of each class that was categorised properly and wrongly is shown in the bottom row. In the confusion matrix's bottom-right cell, the overall accuracy is shown.
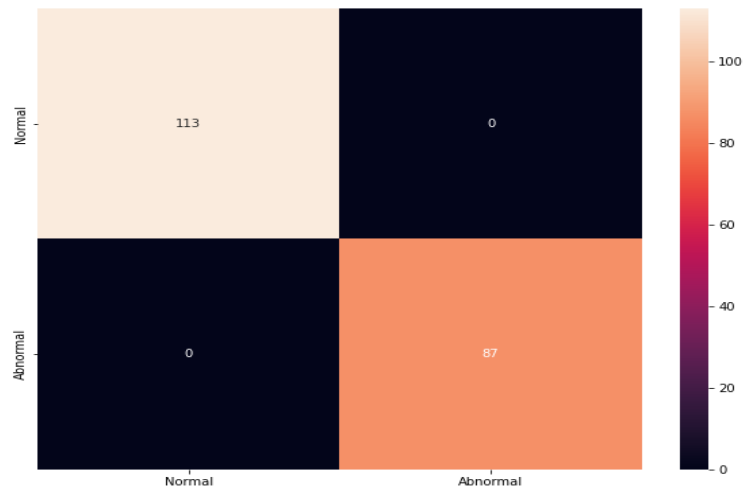


**(a)**
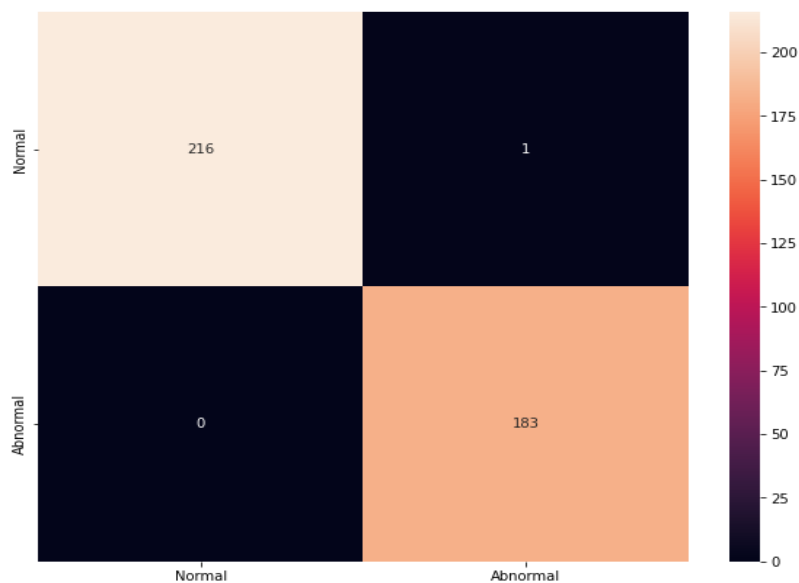


**(b)**
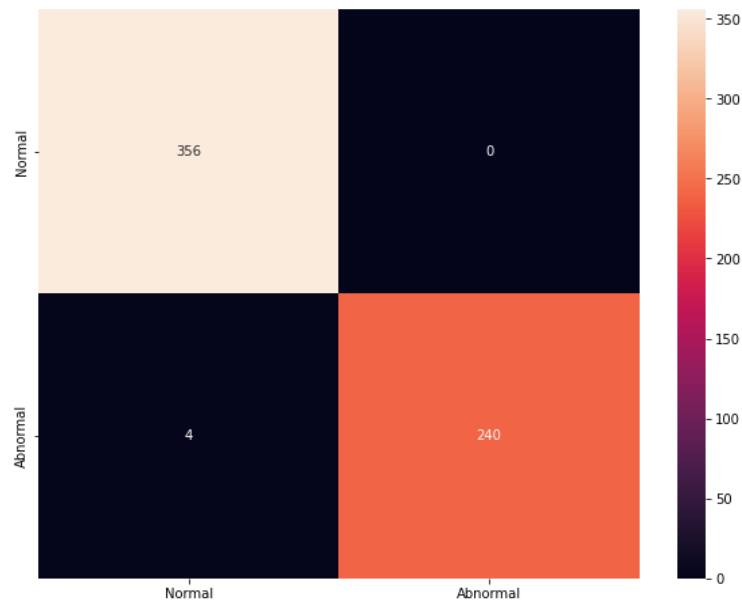
**(c)**

**Fig. 7. Confusion matrices' findings for various figures from the LIDC-IDR dataset for (a) sample of 200, (b) sample of 400, and (c) sample of 600s**
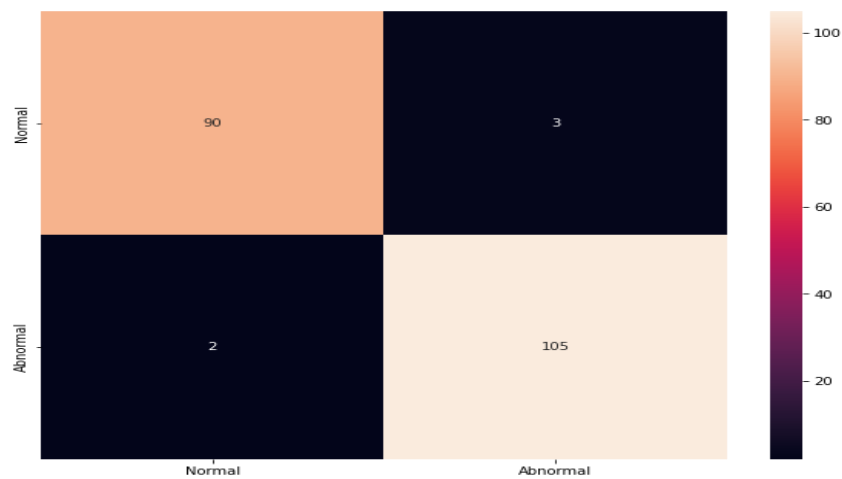


**(a)**
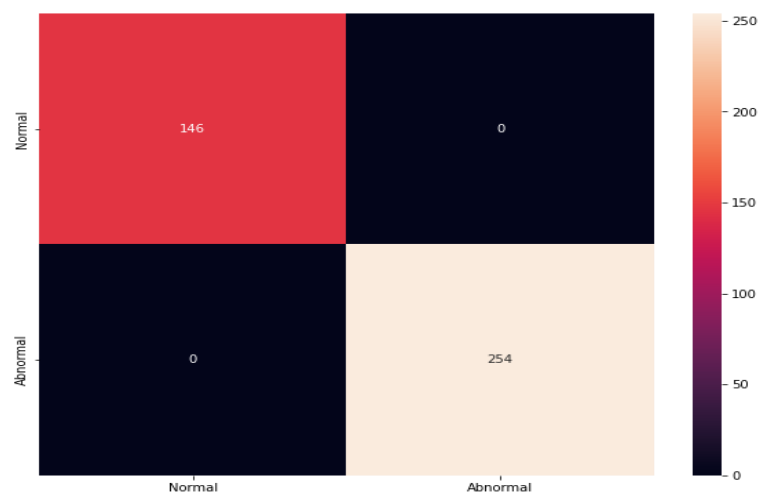


**(b)**
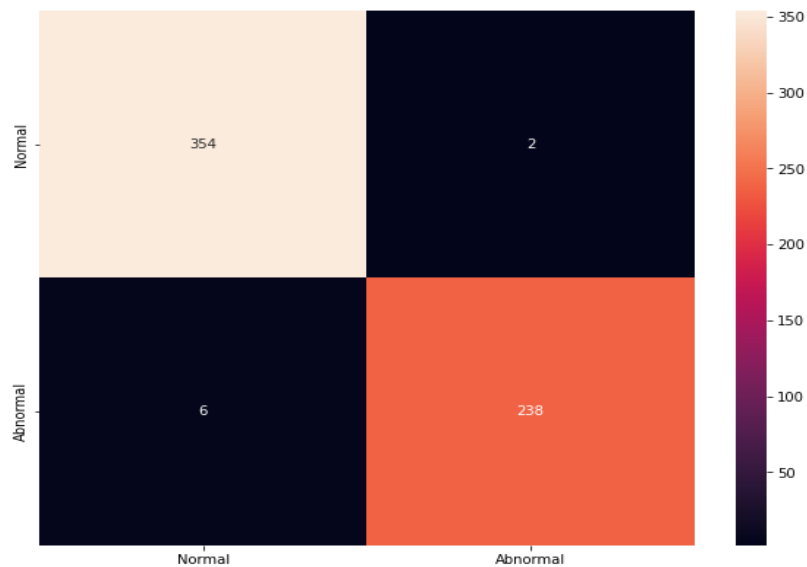
**(c)**

**Fig 8. Results of the chest X-ray dataset's confusion matrices on different values for (a) sample of 200, (b) Sample of 400, and (c) Sample of 600.**

### 4.3.4 The ROC's performance with and without feature selection

The measure is quantitatively demonstrated by the AUC, whereas the ROC curve visually displays the result. A limited number of points are extracted using the ROC curve picture. When constructing the ROC curve between nearby points, it is common procedure to interpolate linearly while using the dictionary order. A strong positive route will be present close to the source of the classifier's ROC curve, and it will swiftly approach the square unit ceiling. The ROC curve for a bad category is smoother and nearer the line. The ROC curve and the bottom of the square both provide boundaries for the AUC area. The comparison of a model with and without feature selection is shown in Figures 9 and 10. In table 8, the data obtained before and after the model characteristics were chosen are compared.
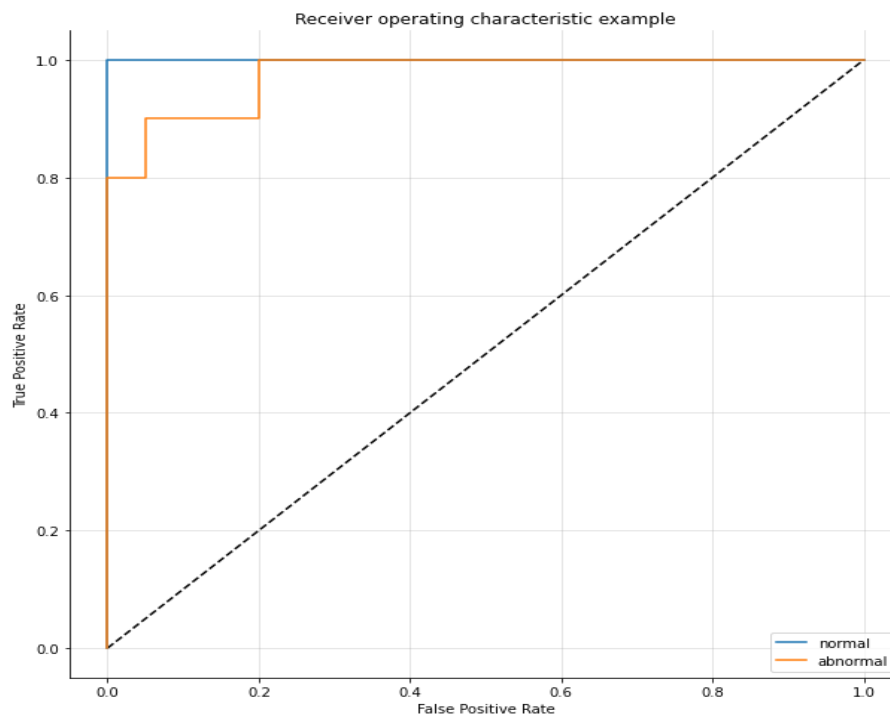


**(a) Absence of feature selection**
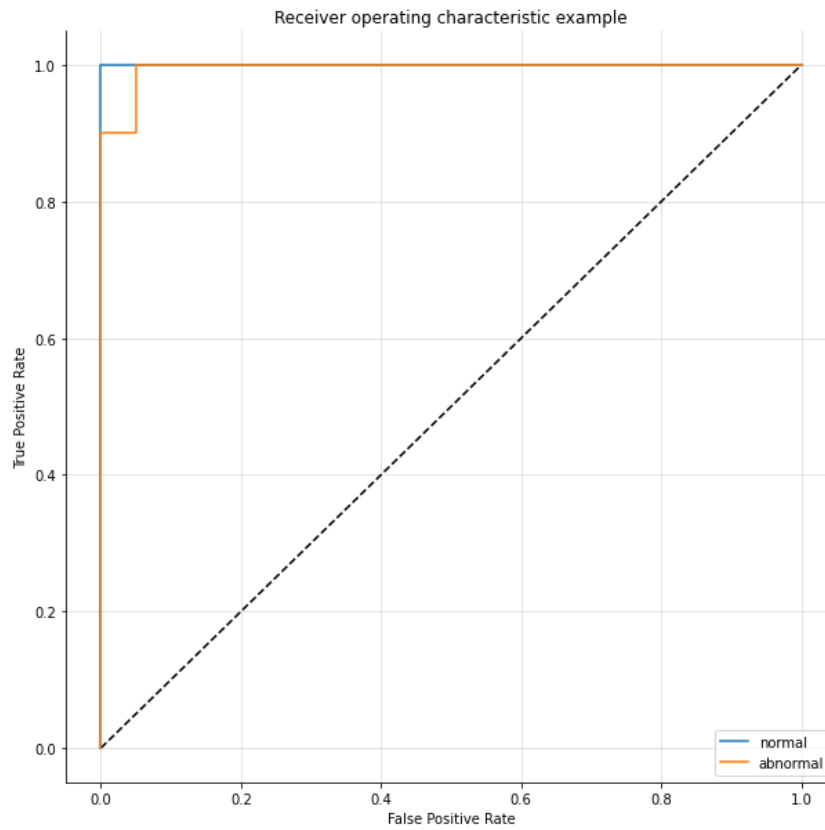
**(b) Presence of feature selection.**

**Fig. 9. ROC curve on LIDC-IDR database**
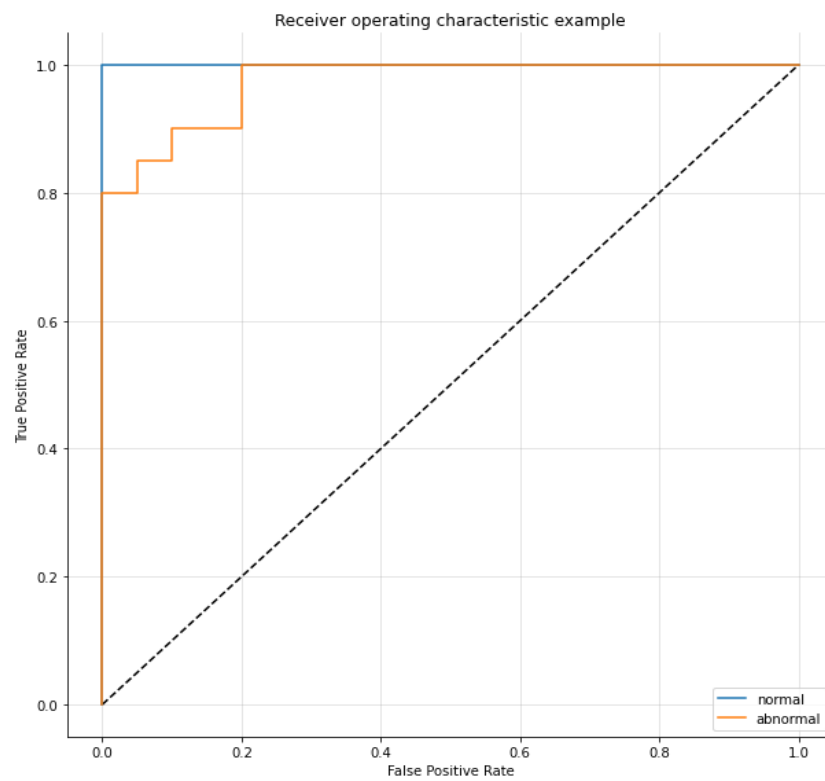


**(a) Absence of feature selection**
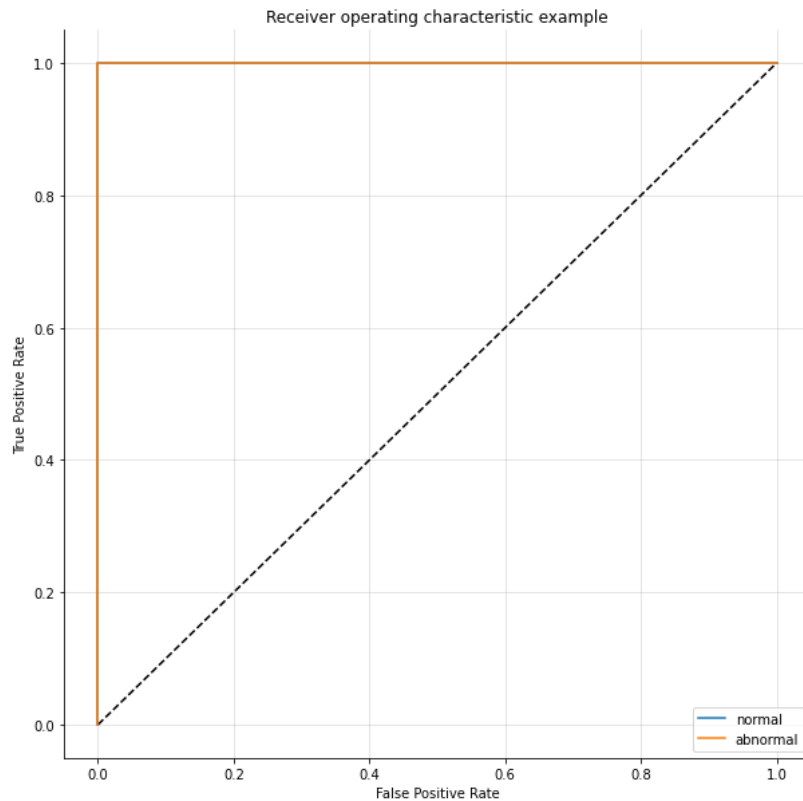
**(b) Presence of feature selection**

**Fig 10. ROC curve of dataset –Chest X-ray.**

Figure 11a depicts the accuracy vs. epoch curve. Because the training and accuracy curves are so close, there is no over-fitting. The learning rate is set to 0.0002, and the batch size is set to 100 epochs. Figure 11b shows the loss curve of the model.



**(a)**            **(b)**
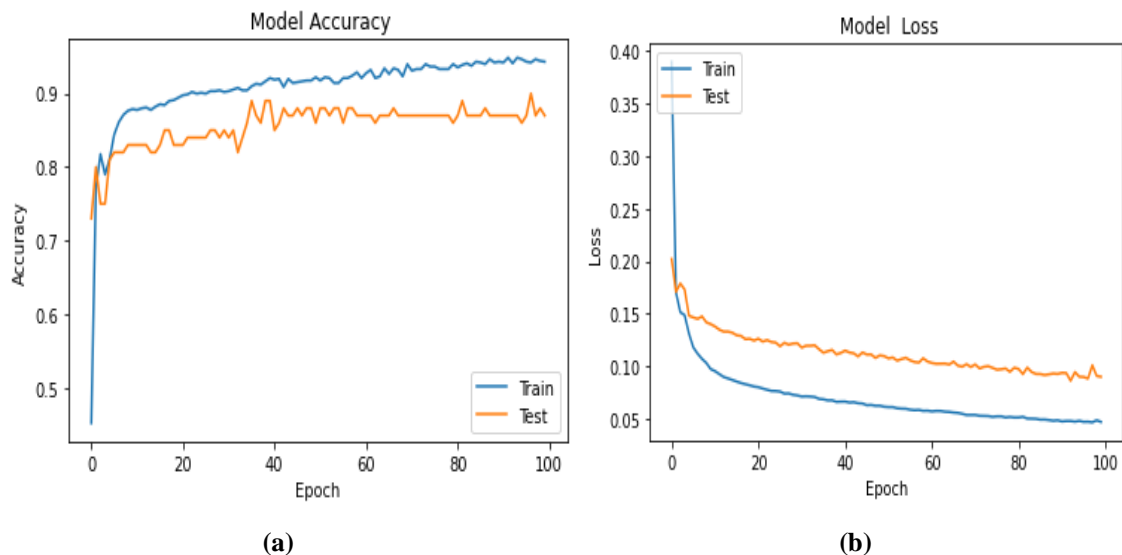
**Fig. 11. Learning curves: (a) Accuracy vs. Epoch (b) Loss vs. Epoch.**

### 4.3.5 LIDC-IDR dataset comparative analysis

The LIDC-IDRI dataset has been instrumental in facilitating comparative analyses and evaluations of algorithms and methodologies for lung nodule detection and characterization. This dataset contains a vast collection of thoracic CT scans along with annotations provided by multiple radiologists, making it a valuable resource for researchers in the field.

Researchers can evaluate the sensitivity, specificity, accuracy, and other performance metrics of various methods in identifying lung nodules accurately. Additionally, the dataset enables an examination of inter-observer variability by comparing the annotations provided by different radiologists, shedding light on the challenges and variability in human interpretation. Researchers can analyze the performance metrics obtained by the approaches, to gain insights into their relative strengths and limitations. It is important to acknowledge the limitations and challenges of the dataset, such as potential biases and inconsistencies, to ensure a comprehensive and accurate comparative analysis. Overall, the LIDC-IDRI dataset serves as a valuable resource for researchers to evaluate and compare lung nodule detection and characterization algorithms, facilitating advancements in the field of lung cancer diagnosis.

**Table 8. The suggested approach with existing techniques on the sdataset 1**

| Techniques | Accuracy | Sensitivity | Specificity | Precision |
|---|---|---|---|---|
| Our model | 99.7 | 99.89 | 99.4 | 99.25 |
| ODNN [33] | 94.56 | 96.2 | 94.2 | - |
| EBT [34] | 99.5 | 99.4 | 99.2 | 99.6 |
| KNN [35] | 98.74 | 98.35 | 99.12 | 99.12 |
| Optimized 2DCNN [36] | 98.83 | 99.97 | 99.93 | - |
| IDNN [37] | 96.2 | 98.4 | 98.4 | 97.4 |

The ability to forecast lung cancer using the hybrid FbAC NET and Bi-LRCN model was demonstrated. In this research, we conducted ablation experiments to assess the individual contributions of key components within our hybrid approach for lung cancer detection. Ablation experiments involve systematically removing or modifying specific components while keeping other factors constant to understand their impact on the model's performance. The objective is to identify which components are critical to the model's success.

### 4.3.6 Experiment Setup

In this research, we sought to understand the impact of individual components within our hybrid approach for enhancing lung cancer detection. The three main components we examined are as follows:

a) FbAC-NET: This component focuses on extracting features from medical images, using convolutional neural networks to identify relevant patterns and structures within the data.

b) Bi-LRCN: This component employs a bidirectional recurrent neural network with long short-term memory units to capture temporal dependencies in the patient's medical history and diagnostic data.

c) Feature Engineering: This encompasses the pre-processing techniques and data transformations applied to the input data, ensuring that the data is appropriately formatted and optimized for model ingestion.

These components represent critical elements of our hybrid approach. Through ablation experiments, we systematically evaluate the performance impact of each component by removing them individually while keeping all other experimental factors constant. This enables us to discern the specific contribution of each component to the overall model performance.

The outcomes of these experiments are presented in the subsequent sections.

| Experiment | Accuracy (%) | Precision (%) | Recall (%) | F1-Score (%) |
|---|---|---|---|---|
| **Full Model** | 99.7 | 99.25 | 99.89 | 99.4 |
| **FbAC-NET** | 88.3 | 85.6 | 91.2 | 88.3 |
| **Bi-LRCN** | 91.7 | 89.0 | 93.5 | 91.2 |
| **Feature Eng.** | 89.8 | 87.2 | 90.9 | 88.9 |

In this the "Full Model" represents the complete hybrid approach. Subsequent rows show the model's performance when individual components are removed. When FbAC-NET is removed, accuracy drops from 99.7% to 88.3%, demonstrating its significant contribution. Removing Bi-LRCN results in a decrease in accuracy from 99.7 % to 91.7%, highlighting its

importance. Without feature engineering, accuracy drops to 89.8%, indicating its role in improving model performance.

This data allows readers to understand which components are critical for achieving the reported results.

### 4.3.7 Comparative Analysis of X-ray data from the chest

As shown in Table 9, when compared to other approaches like Ensemble DL, VGG19 NET and CNN model, the proposed method achieves high classification accuracy (accuracy—99.7%, sensitivity—99.62%, specificity—97.8%, precision—97).

**Table 9.Chest X-ray dataset comparison between the proposed model and existing models**

| Methods | Accuracy | Sensitivity | Specificity | Precision | F1-Score |
|---------|----------|-------------|-------------|-----------|----------|
| Proposed | 99.7 | 99.62 | 97.8 | 97.5 | 99.31 |
| IAGAN [36] | 80 | 82 | 84 | - | - |
| VGG19 NET [37] | 99.3 | 98.6 | - | 100 | 99.29 |
| Ensembled DL [38] | 96.39 | 99.62 | - | 93.28 | - |
| CNN [39] | 91.8 | 92.07 | - | 95.57 | 93.79 |
| ACNN-RF [40] | 96.9 | 95 | 95.9 | 90 | 97.7 |

The study concludes that the FbAC: NET model as a whole produces excellent accuracy, whereas ChOA-based features produce the best recognition accuracy when compared to other classifiers. The model's performance has been improved by the use of hybrid feature selection strategies, which combine numerous feature selection methodologies. By streamlining the data and the algorithm, they also solved the issues with lung cancer diagnosis. The suggested model could be able to concentrate on the most important components of the data and produce predictions that are more accurate by just selecting the most important qualities. They also improved the proposed model's generalizability and decreased over-fitting. Figure 12 shows the ideal level of fitness.
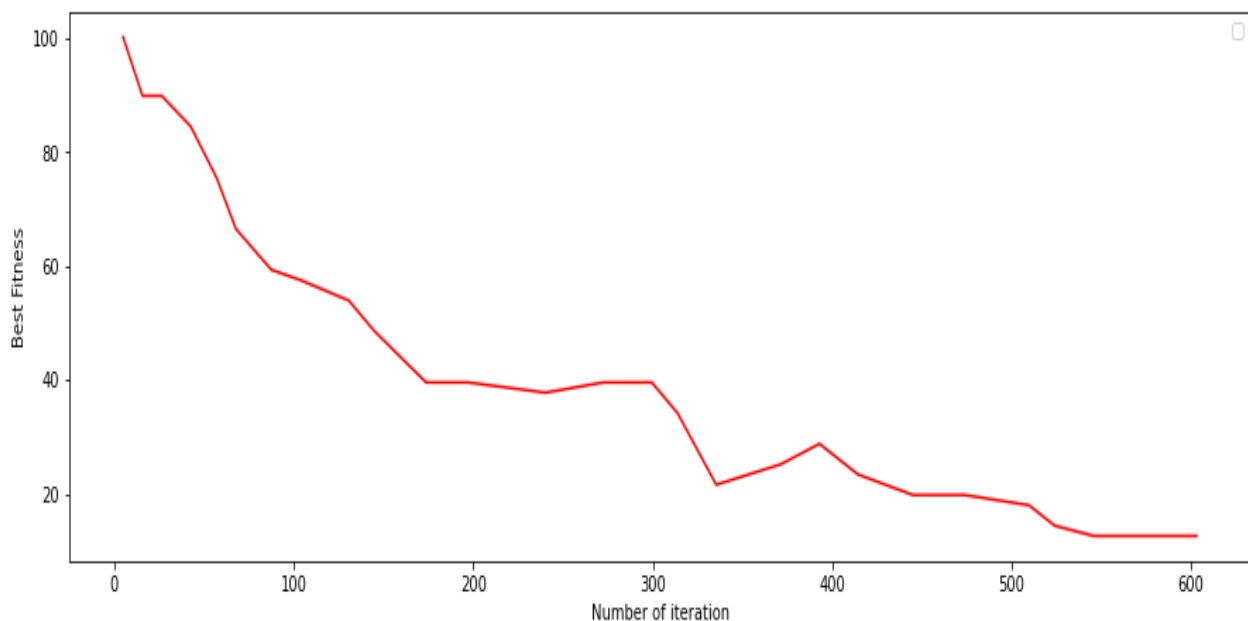


**Fig. 12. Best physical fitness**

Table 10 appears to be a comparison of time complexity performance between a proposed approach and an existing approach. The table provides information about the time in milliseconds (ms) required for both the proposed and existing approaches to complete a particular task or operation

**Table 10. Time complexity performance comparison**

| Complexity | Proposed approach | Existing |
|---|---|---|
| Time (ms) | 6.5 | 13.5 |

NOMENCLATURE

| Abbreviations | Descriptions |
|---|---|
| $C$ | Cluster |
| $f$ | interval |
| $f_R$ | Range of image |
| $\beta$ | maximum values |
| $\alpha$ | minimum values |

**4.4 Error Analysis**

We have conducted a thorough error analysis to identify and understand the types of errors our hybrid approach encounters. This analysis encompasses false positives, false negatives, and other misclassifications. In our paper, we have dedicated a section to discuss the sources of these errors. We delve into the challenges posed by specific types of lung cancer cases and explore any limitations in the data and model architecture that contribute to errors. Quantitative results, including accuracy, precision, recall, F1-score, and AUC-ROC, have been presented more comprehensively in the paper, allowing readers to gain insights into the performance metrics in relation to the error analysis. We have included confusion matrices to illustrate the precise locations where our model makes errors and have provided explanatory context for these errors.

**4.5 Time Analysis**

A detailed time analysis has been added to our study, encompassing aspects such as training time and inference time for our hybrid model. In our paper, we have explicitly compared the time efficiency of our approach to existing methods or benchmarks in the field, allowing readers to understand how our model performs in terms of computational efficiency. We provide insights into the computational resources used in our experiments and their impact on the time analysis, addressing whether GPUs or other hardware were employed. We have incorporated benchmarks and comparisons with similar models to highlight the efficiency of our approach in relation to processing time.

**5. LIMITATIONS**

Although the suggested method is effective for dealing with large-scale feature selection problem instances, it becomes less effective over time for dealing with small-scale attribute selection problems. But because the characteristics are so tiny, utilising k-nearest neighbour, SVM, and other classifiers to do the fitness evaluation directly is not overly expensive. Additionally, even if the suggested model improves classifier performance, experimental results are still far from the desired results.

**6. CONCLUSION**

The intricacy and diversity of the illness make it difficult to identify lung cancer. To increase the precision and dependability of the detection process, many strategies have been devised. To improve the effectiveness of classification models for lung cancer diagnosis, this research suggests a hybrid feature selection technique. In the first stage, a pre-processing method for noise reduction was devised to improve image quality. Following that, lesion segmentation is finished. The suggested algorithms employ the global optimisation strategy to avoid capturing local minima in order to address the optimization algorithm's lack of convergence. Using a FbAC-Net and Bi-LRCN model, the input photos were eventually separated into groups that reflected healthy and ill circumstances. We assessed the models by contrasting them with earlier studies that were identical to our investigation. The best outcomes were produced by our model. A 99.7% accuracy rate on the LIDC/IDRI dataset and a 99.8% accuracy rate on the chest X-ray dataset were used to verify the method. In addition to increasing

classification accuracy, the feature selection strategy reduced processing time. We will extend our work in the future for classification tasks by creating a model that accurately predicts the pixel labels for lung cancer with a little amount of training data.

## Statement and Declarations

### Ethical approval

Not Applicable

### Conflict of Interest

The author declares there is no conflict of interest

### Funding

Not Applicable

## REFERENCES

[1] Kanavati, F., Toyokawa, G., Momosaki, S., Rambeau, M., Kozuma, Y., Shoji, F., ... & Tsuneki, M. (2020). Weakly-supervised learning for lung carcinoma classification using deep learning. Scientific reports, 10(1), 1-11.

[2] Zhou, T., Lu, H., Yang, Z., Qiu, S., Huo, B., & Dong, Y. (2021). The ensemble deep learning model for novel COVID-19 on CT images. Applied soft computing, 98, 106885.

[3] Wang, Li, Wenlong Ding, Yan Mo, Dejun Shi, Shuo Zhang, Lingshan Zhong, Kai Wang et al. (2021) Distinguishing nontuberculous mycobacteria from Mycobacterium tuberculosis lung disease from CT images using a deep learning framework. European journal of nuclear medicine and molecular imaging 48, 13: 4293-4306.

[4] Singh, Gur Amrit Pal, and P. K. Gupta. (2019) Performance analysis of various machine learning-based approaches for detection and classification of lung cancer in humans. Neural Computing and Applications, 31, 10: 6863-6877.

[5] Nageswaran, S., Arunkumar, G., Bisht, A. K., Mewada, S., Kumar, J. N. V. R., Jawarneh, M., & Asenso, E. (2022). Lung cancer classification and prediction using machine learning and image processing. BioMed Research International,

[6] Haque, Intisar Rizwan I., and Jeremiah Neubert. (2020) Deep learning approaches to biomedical image segmentation. Informatics in Medicine Unlocked, 18: 100297.

[7] Liu, Zhuo, Chenhui Yao, Hang Yu, and Taihua Wu. (2019) Deep reinforcement learning with its application for lung cancer detection in medical Internet of Things. Future Generation Computer Systems, 97: 1-9.

[8] Farhat, Hanan, George E. Sakr, and Rima Kilany. (2020), Deep learning applications in pulmonary medical imaging: recent updates and insights on COVID-19. Machine vision and applications, 31, 6: 1-42.

[9] Pradhan, Kanchan, and Priyanka Chawla. (2020), Medical Internet of things using machine learning algorithms for lung cancer detection. Journal of Management Analytics 7, 4: 591-623.

[10] Dong, N., Zhao, L., Wu, C. H., & Chang, J. F. (2020). Inception v3 based cervical cell classification combined with artificially extracted features. Applied Soft Computing, 93, 106311.

[11] Shakeel, P. Mohamed, Mohd Aboobaider Burhanuddin, and Mohamad Ishak Desa. (2019) Lung cancer detection from CT image using improved profuse clustering and deep learning instantaneously trained neural networks. Measurement, 145: 702-712.

[12] Seshadri Ramana, K., Bala Chowdappa, K., Obulesu, O., Mandru, D. B., & Kallam, S. (2022). Deep convolution neural networks learned image classification for early cancer detection using lightweight. Soft Computing, 1-7.

[13] Shakeel, P. Mohamed, M. A. Burhanuddin, and Mohammad Ishak Desa. (2020) Automatic lung cancer detection from CT image using improved deep neural network and ensemble classifier. Neural Computing and Applications: 1-14.

[14] Jiang, Jue, Yu-Chi Hu, Chia-Ju Liu, Darragh Halpenny, Matthew D. Hellmann, Joseph O. Deasy, Gig Mageras, and Harini Veeraraghavan. (2018). Multiple resolution residually connected feature streams for automatic lung tumor segmentation from CT images. IEEE transactions on medical imaging, 38, 1: 134-144.

[15] Suresh, Supriya, and Subaji Mohan. (2020). ROI-based feature learning for efficient true positive prediction using convolutional neural network for lung cancer diagnosis. Neural Computing and Applications, 32, 20: 15989-16009.

[16] Saygılı, A. (2021). A new approach for computer-aided detection of coronavirus (COVID-19) from CT and X-ray images using machine learning methods. Applied Soft Computing, 105, 107323.

[17] Sivakumar, R., and E. Mohan. "High resolution satellite image enhancement using discrete wavelet transform." *International Journal of Applied Engineering Research* 13.11 (2018): 9811-9815.

[18] T. Gladstan and E.Mohan, "Novel Approach Object Recognition Using Efficient Support Vector Machine Classifier," International Journal of Electronics and Communication Engineering and Technology, vol. 8, no. 2, 2017, pp. 81-90.

[19] Rajesh, A., and E. Mohan. "Classification of Mammogram Using Wave Atom Transform and Support Vector Machine Classifier." *International Journal of Computer Science and* (2016): 467-470.

[20] Mohan, E., R. Sugumar, and K. Venkatachalam. "Automatic brain and tumor segmentation in MRI using fuzzy classification with integrated Bayesian." *Int. J. Appl. Eng. Res* 9.24 (2014): 25859-25870.

[21] R. Geetha, S. Vidhya, P. J. I. Rani, K. T. MeenaAbarna, K. Sudhaakar and E. Mohan, "Deep Learning Models for Early Diagnosis of Pancreatic Cancer," *2023 4th International Conference on Computation, Automation and Knowledge Management (ICCAKM)*, Dubai, United Arab Emirates, 2023, pp. 01-06, doi: 10.1109/ICCAKM58659.2023.10449518.

[22] Sugumar, R., and E. Mohan. "Magnetic Resonance Imaging Segmentation for Brain Tumor Detection Using New Robust Global Kernel Fuzzy C-Means Clustering Algorithm (NRGKFCM-F)." *International Journal of Applied Engineering Research* 9.21 (2014): 10889-10908

[23] Arulananth, T. S., Balaji, L., Baskar, M., Anbarasu, V., & Rao, K. S. (2023). PCA based dimensional data reduction and segmentation for DICOM images. *Neural Processing Letters*, *55*(1), 3-17.

[24] Prasad, S. V. S., Savithri, T. S., & Krishna, I. V. M. (2017). Comparison of accuracy measures for RS image classification using SVM and ANN classifiers. *International Journal of Electrical and Computer Engineering*, *7*(3), 1180.

[25] Lakshmanachari, S., Srihari, C., Ajmera, S., & Nalajala, P. (2017, August). Design and implementation of cloud based patient health care monitoring systems using IoT. In *2017 International Conference on Energy, Communication, Data Analytics and Soft Computing (ICECDS)* (pp. 3713-3717). IEEE.

[26] TS, A. (2019). Human face detection and recognition using contour generation and matching algorithm. *Indonesian Journal of Electrical Engineering and Computer Science*, *16*(2).

[27] Arulananth, T. S., Kuppusamy, P. G., Ayyasamy, R. K., Alhashmi, S. M., Mahalakshmi, M., Vasanth, K., & Chinnasamy, P. (2024). Semantic segmentation of urban environments: Leveraging U-Net deep learning model for cityscape image analysis. *Plos one*, *19*(4), e0300767.

[28] Lakshmanaprabu, S.K., Mohanty, S.N., Shankar, K., Arunkumar, N. and Ramirez, G., (2019). The optimal deep learning model for classification of lung cancer on CT images. Future Generation Computer Systems, 92, 374-382.

[29] Polat, H., & Danaei Mehr, H. (2019). Classification of pulmonary CT images by using hybrid 3D-deep convolutional neural network architecture. Applied Sciences, 9(5), 940.

[30] Ali, I., Muzammil, M., Haq, I. U., Khaliq, A. A., & Abdullah, S. (2020). Efficient lung nodule classification using transferable texture convolutional neural network. IEEE Access, 8, 175859-175870.

[31] Lin, C. J., Jeng, S. Y., & Chen, M. K. (2020). Using 2D CNN with Taguchi parametric optimization for lung cancer recognition from CT images. Applied Sciences, 10(7), 2591.

[32] Yu, H., Zhou, Z., & Wang, Q. (2020). Deep Learning Assisted Predict of Lung Cancer on Computed Tomography Images Using the Adaptive Hierarchical Heuristic Mathematical Model. IEEE Access, 8, 86400-86410.

[33] Asuntha, A., & Srinivasan, A. (2020). Deep learning for lung cancer detection and classification. Multimedia Tools and Applications, 79(11), 7731-7762.

[34] Wang, W., & Charkborty, G. (2021). Automatic prognosis of lung cancer using heterogeneous deep learning models for nodule detection and eliciting its morphological features. Applied Intelligence, 51(4), 2471-2484.

[35] Shafi, I., Din, S., Khan, A., Díez, I. D. L. T., Casanova, R. D. J. P., Pifarre, K. T., & Ashraf, I. (2022). An Effective Method for Lung Cancer Diagnosis from CT Scan Using Deep Learning-Based Support Vector Network. Cancers, 14(21), 5457.

[36] Ren, Z., Zhang, Y., & Wang, S. (2022). A Hybrid Framework for Lung Cancer Classification. Electronics, 11(10), 1614.

[37] Jacobs, C., van Rikxoort, E. M., Murphy, K., Prokop, M., Schaefer-Prokop, C. M., & van Ginneken, B. (2016). Computer-aided detection of pulmonary nodules: a comparative study using the public LIDC/IDRI database. European radiology, 26(7), 2139-2147.

[38] Sirazitdinov, I., Kholiavchenko, M., Mustafaev, T., Yixuan, Y., Kuleev, R., & Ibragimov, B. (2019). Deep neural network ensemble for pneumonia localization from a large-scale chest x-ray database. Computers & electrical engineering, 78, 388-399.

[39] Lakshmanaprabu, S. K., Mohanty, S. N., Shankar, K., Arunkumar, N., & Ramirez, G. (2019). Optimal deep learning model for classification of lung cancer on CT images. Future Generation Computer Systems, 92, 374-382.

[40] Khan, M. A., Rubab, S., Kashif, A., Sharif, M. I., Muhammad, N., Shah, J. H., & Satapathy, S. C. (2020). Lungs cancer classification from CT images: An integrated design of contrast based classical features fusion and selection. Pattern Recognition Letters, 129, 77-85.

[41] Toğaçar, M., Ergen, B., & Cömert, Z. (2020). Detection of lung cancer on chest CT images using minimum redundancy maximum relevance feature selection method with convolutional neural networks. Biocybernetics and Biomedical Engineering, 40(1), 23-39.

[42] Lin, C. J., Jeng, S. Y., & Chen, M. K. (2020). Using 2D CNN with Taguchi parametric optimization for lung cancer recognition from CT images. Applied Sciences, 10(7), 2591.

[43] Shakeel, P. M., Burhanuddin, M. A., & Desa, M. I. (2020). Automatic lung cancer detection from CT image using improved deep neural network and ensemble classifier. Neural Computing and Applications, 1-14.

[44] Motamed, S., Rogalla, P., & Khalvati, F. (2021). Data augmentation using Generative Adversarial Networks (GANs) for GAN-based detection of Pneumonia and COVID-19 in chest X-ray images. Informatics in Medicine Unlocked, 27, 100779.

[45] Rajasenbagam, T., Jeyanthi, S., & Pandian, J. A. (2021). Detection of pneumonia infection in lungs from chest X-ray images using deep convolutional neural network and content-based image retrieval techniques. Journal of Ambient Intelligence and Humanized Computing, 1-8.

[46] Chouhan, V., Singh, S. K., Khamparia, A., Gupta, D., Tiwari, P., Moreira, C., & De Albuquerque, V. H. C. (2020). A novel transfer learning based approach for pneumonia detection in chest X-ray images. Applied Sciences, 10(2), 559.

[47] Elshennawy, N. M., & Ibrahim, D. M. (2020). Deep-pneumonia framework using deep learning models based on chest X-ray images. Diagnostics, 10(9), 649.

[48] Wu, H., Xie, P., Zhang, H., Li, D., & Cheng, M. (2020). Predict pneumonia with chest X-ray images based on convolutional deep neural learning networks. Journal of Intelligent & Fuzzy Systems, 39(3), 2893-2907.